Applied Energy 225 (2018) 637–655

Contents lists available at ScienceDirect

Applied Energy

journal homepage: www.elsevier.com/locate/apenergy

Finite-rate chemistry modelling of non-conventional combustion regimes using a Partially-Stirred Reactor closure: Combustion model formulation and implementation details☆

Zhiyi Li[a,b], Marco Ferrarotti[a,b,c], Alberto Cuoci[d], Alessandro Parente[a,b,*]

[a] Université Libre de Bruxelles, Ecole Polytechnique de Bruxelles, Aero-Thermo-Mechanics Laboratory, Brussels, Belgium
[b] Université Libre de Bruxelles and Vrije Universiteit Brussel, Combustion and Robust Optimization Group (BURN), Brussels, Belgium
[c] Service de Thermique et Combustion, Université de Mons, Mons, Belgium
[d] Department of Chemistry, Materials, and Chemical Engineering, Politecnico di Milano, Piazza Leonardo da Vinci, 20133 Milano, Italy

HIGHLIGHTS

- A study on the advanced Moderate or Intense Low oxygen Dilution combustion technology.
- A comprehensive analysis on different time scales in Partially-Stirred Reactor model.
- Consideration of wide range of operation conditions for model validation.
- Obviously improved simulation accuracy.

ARTICLE INFO

Keywords:
Characteristic time scales
Chemical time scale
Finite-rate chemistry
MILD combustion
Mixing time scale
Partially-Stirred Reactor

ABSTRACT

The present work focuses on the numerical simulation of Moderate or Intense Low oxygen Dilution combustion condition, using the Partially-Stirred Reactor model for turbulence-chemistry interactions. The Partially-Stirred Reactor model assumes that reactions are confined in a specific region of the computational cell, whose mass fraction depends both on the mixing and the chemical time scales. Therefore, the appropriate choice of mixing and chemical time scales becomes crucial to ensure the accuracy of the numerical simulation prediction. Results show that the most appropriate choice for mixing time scale in Moderate or Intense Low oxygen Dilution combustion regime is to use a dynamic evaluation, in which the ratio between the variance of mixture fraction and its dissipation rate is adopted, rather than global estimations based on Kolmogorov or integral mixing scales. This is supported by the validation of the numerical results against experimental profiles of temperature and species mass fractions, available from measurements on the Adelaide Jet in Hot Co-flow burner. Different approaches for chemical time scale evaluation are also compared, using the species formation rates, the reaction rates and the eigenvalues of the formation rate Jacobian matrix. Different co-flow oxygen dilution levels and Reynolds numbers are considered in the validation work, to evaluate the applicability of Partially-Stirred Reactor approach over a wide range of operating conditions. Moreover, the influence of specifying uniform and non-uniform boundary conditions for the chemical scalars is assessed. The present work sheds light on the key mechanisms of turbulence-chemistry interactions in advanced combustion regimes. At the same time, it provides essential information to advance the predictive nature of computational tools used by scientists and engineers, to support the development of new technologies.

1. Introduction

Recently, the reduction of fossil fuel availability and the increasing environmental concerns associated to their utilization in conventional systems have pushed the development of new combustion technologies that feature high fuel flexibility, increased efficiency and low pollution emissions. Among them, Moderate or Intense Low oxygen Dilution (MILD) combustion [1,2] has recently drawn increasing attention. MILD combustion is characterized by elevated reactant temperature and low temperature increase [1,3], intensive reactant and product

☆ The short version of the paper was presented at ICAE2017, Aug 21–24, Cardiff, UK. This paper is a substantial extension of the short version of the conference paper.

* Corresponding author at: Université Libre de Bruxelles, Ecole Polytechnique de Bruxelles, Aero-Thermo-Mechanics Laboratory, Brussels, Belgium.
E-mail address: Alessandro.Parente@ulb.ac.be (A. Parente).

https://doi.org/10.1016/j.apenergy.2018.04.085
Received 3 January 2018; Received in revised form 13 April 2018; Accepted 27 April 2018
Available online 26 May 2018

mixing, as well as no audible or visible flame, under ideal conditions. Moreover, MILD combustion delivers very low NO_x and CO emissions and high efficiency, with a large flexibility of fuel types [2,4].

MILD combustion technology has been demonstrated for many industrial applications. It was first introduced in industrial furnaces for methane combustion [5] and later extensively investigated for other gaseous fuels like hydrogen [6] and ethanol [7]. Cho et al. [8,9] executed experiments and simulations on MILD oxidation burner, showing the effects of burner configuration and firing mode on efficiency and emissions. Sánchez et al. [10] evaluated an oxygen enhanced regenerative burner operated in MILD combustion mode. An energy recovery ratio above 80% and NO_x emissions below 5 ppm were achieved. Ye et al. [11] studied prevaporised liquid fuels burning in a reverse-flow MILD combustor under elevated pressures. They concluded that combustion stability is largely dependent on fuel type and the NO_x emission is highly influenced by the operating conditions of pressure, jet velocity and carrier gas. MILD technology can be utilized in gas turbines as well. Kruse et al. [12] conducted experimental and numerical studies on gas turbine under MILD condition, using gaseous fuel. The effect of pressure, mixing on combustion stability was analysed, indicating that mixing is the key parameter to control and stabilize MILD combustion. Recently, Xing et al. [7] evaluated the possibility of using liquid biofuels, diesel and kerosene fuels under MILD condition for gas turbine applications. They stated that MILD combustion can potentially substitute conventional gas turbines. Furthermore, Adamczyk et al. [13] analysed the potential of oxy-MILD combustion for large scale pulverized coal boilers. Preliminary simulations showed the possibility of efficiency increase of more than 3%. The MILD combustion concept was also extended to hybrid solar thermal devices, which combine concentrated solar radiation with combustion. According to Chinnici et al. [14], the integration of MILD combustion in a hybrid solar receiver can lead to increased thermal performances with respect to conventional flames.

The distinguishing feature of MILD combustion is the very strong interactions between the fluid mixing and chemical kinetics, so that models based on the separation between turbulence and chemistry are not suitable to describe the complex interactions occurring in such a regime [15]. Therefore, models that account for finite-rate chemistry effects must be considered. The present study focuses on Unsteady Reynolds Averaged Navier-Stokes (URANS) simulations in combination with finite-rate chemistry. The Partially-Stirred Reactor (PaSR) model [16] is chosen for turbulence/chemistry interactions. In PaSR, the interaction between turbulence and chemistry is represented with a factor κ, which is defined as the ratio between the chemical time scale and the sum of mixing and chemical scales. PaSR models the combustion process as a sequence of reaction and mixing processes in locally uniform regions. Both the chemical and mixing time scales are included in the model explicitly, allowing more comprehensive descriptions on turbulence/chemistry interactions. Therefore, its performances strongly depend on the accurate estimation of mixing and chemical time scales.

Regarding the evaluation of chemical and mixing time scales, Chomiak [17] estimated the chemical time scale using the fuel and oxidiser formation rates, and the mixing time from the geometric mean of integral and komogorov mixing time scales. Golovitchev et al. [18] proposed an approach in which the chemical time scale is estimated from forward reaction rates only. Kärrholm [19] and Nordin [20] estimated the mixing time scale as a certain fraction of the integral one, using a mixing constant C_{mix} ranging from 0.001 to 0.3 [20]. To the best of the authors' knowledge, no study was carried out to compare the available approaches for mixing and chemical time scale evaluation.

The objective of the present article is to provide a comprehensive analysis on existing and novel approaches for the evaluation of chemical and mixing time scales and boundary conditions in the framework of finite-rate chemistry approach for turbulent reacting flows. The available models are benchmarked in the context of MILD combustion simulations under a wide range of operation conditions. A cross-comparison between an open-source CFD software OpenFOAM and a commercial one, ANSYS Fluent 17.0 [21], is also carried out, to show the applicability of the proposed methodology on different computing platforms.

Numerical simulations are validated against high-fidelity experimental results available from the Adelaide Jet in Hot Co-flow (AJHC) burner [22]. The AJHC burner emulates MILD conditions via the injection of a heated and vitiated co-flow. Measurement data for different co-flow oxygen levels (3%, 6% and 9%) and fuel jet Reynolds numbers (5 k, 10 k and 20 k) are available. The AJHC burner with 3% co-flow oxygen content and $Re = 10\,k$ is chosen first for the evaluation of various mixing time scale and chemical time scale formulations. The best combination of mixing and chemical scales is then used for the other co-flow oxygen levels and Reynolds numbers. Finally, the influence of uniform and non-uniform boundary conditions on the model prediction is assessed, paying particular attention to carbon monoxide prediction.

2. Methodology

The Finite Volume Method (FVM) based URANS simulations are carried out with PaSR combustion model.

2.1. Turbulence model

In the context of compressible URANS simulations, the Favre-averaged (denoted with ˜) governing equations are solved [23]:

$$\frac{\partial \overline{\rho}}{\partial t} + \frac{\partial}{\partial x_j}(\overline{\rho}\widetilde{u}_j) = 0, \tag{1}$$

$$\frac{\partial}{\partial t}(\overline{\rho}\widetilde{u}_i) + \frac{\partial}{\partial x_j}(\overline{\rho}\widetilde{u}_i\widetilde{u}_j) = -\frac{\partial \overline{p}}{\partial x_i} + \frac{\partial}{\partial x_j}(\overline{\tau}_{ij} - \overline{\rho}\widetilde{u_i''u_j''}), \tag{2}$$

$$\frac{\partial}{\partial t}(\overline{\rho}\widetilde{h}) + \frac{\partial}{\partial x_j}(\overline{\rho}\widetilde{h}\widetilde{u}_j) = \frac{\partial}{\partial x_j}\left(\overline{\rho}\alpha\frac{\partial \widetilde{h}}{\partial x_j} - \overline{\rho}\widetilde{u_j''h''}\right) - \frac{\partial}{\partial x_j}(\overline{q}_r) + \overline{S}_{hc}, \tag{3}$$

$$\frac{\partial}{\partial t}(\overline{\rho}\widetilde{Y}_i) + \frac{\partial}{\partial x_j}(\overline{\rho}\widetilde{Y}_i\widetilde{u}_j) = \frac{\partial}{\partial x_j}\left(\left(\overline{\rho}D_{m,i} + \frac{\mu_t}{Sc_t}\right)\frac{\partial \widetilde{Y}_i}{\partial x_j}\right) + \overline{\omega}_i. \tag{4}$$

In Eqs. (1)–(4), ρ, $\mathbf{u}$, p are the density, velocity and pressure, respectively; h and α represent the enthalpy and thermal diffusivity; Sc_t and $D_{m,i}$ denote the turbulent Schmidt number and molecular diffusion coefficient for species i in the mixture. The standard $k-\epsilon$ model is chosen as turbulence model. It is based on the eddy viscosity assumption. The unresolved turbulence stresses $\overline{\rho}\widetilde{u_i''u_j''}$ are modelled with the product of an eddy viscosity μ_t and mean flow strain rate S_{ij}^*. The eddy viscosity μ_t in standard $k-\epsilon$ model is estimated as:

$$\mu_t = \rho C_\mu \frac{\widetilde{k}^2}{\widetilde{\epsilon}}. \tag{5}$$

The turbulence kinetic energy $\widetilde{k}$ and the dissipation rate $\widetilde{\epsilon}$ of the turbulence kinetic energy [23] are solved via two separate transport equations.

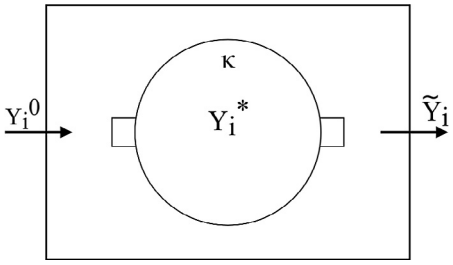

Fig. 1. Conceptual drawing of the PaSR model.

Table 1
Model constants for the scalar dissipation rate transport equations [29].

Case	C_1	C_2	C_3	C_4
1	2.0	1.8	1.7	1.4
2	1.0	1.8	3.4	1.4
3	2.0	1.8	3.4	1.4
4	1.0	1.8	1.7	1.4

2.2. Partially-Stirred Reactor

In the PaSR model [16,18], the computational cell is split into two locally uniform zones: one where reactions take place, and another characterized by only mixing. The final species concentration of the cell is determined from the mass exchange between the two zones, driven by the turbulence. A conceptual drawing of the PaSR model is shown in Fig. 1.

The drawing in Fig. 1 refers to one computational cell, in which Y_i^0 is the initial i_{th} species mass fraction in the non-reactive region, $\widetilde{Y}_i$ is the final averaged i_{th} species mass fraction in the cell and Y_i^* is the i_{th} species mass fraction in the reactive zone. κ is the mass fraction of the reaction zone in the computational cell, which can be estimated as [19]:

$$\kappa = \frac{\tau_c}{\tau_c + \tau_{mix}}, \tag{6}$$

where τ_c and τ_{mix} are the characteristic chemical and mixing time scales in each cell, respectively. They can be estimated following different approaches, as detailed in Sections 2.3 and 2.4. The mean source term provided to the species transport equation can be expressed as:

$$\overline{\dot{\omega}}_i = \kappa \frac{\widetilde{\rho}\,(Y_i^* - Y_i^0)}{\tau^*}, \tag{7}$$

where τ^* represents the residence time in the reactive structure. In the present work, τ^* equals to the mixing time scale. In order to get the value of Y_i^*, a time-splitting approach is applied. The reactive zone is modelled as an ideal reactor evolving from Y_i^0, during a residence time τ^*:

$$\frac{dY_i^*}{dt} = \frac{\dot{\omega}_i}{\rho}. \tag{8}$$

The term $\dot{\omega}_i$ is the instantaneous formation rate of species i. The final integration of $\frac{dY_i^*}{dt}$ over the residence time τ^* in the reactor is Y_i^*.

2.3. Mixing time scale in PaSR

Kolmogorov time scale. In conventional combustion systems, it is often assumed that reactions happen at the dissipation scales, of the order of the Kolmogorov one, $\tau_{mix_K} = \sqrt{\nu/\epsilon}$ [24], where ν is the kinematic viscosity and ϵ is the turbulence kinetic energy dissipation rate. However, in MILD combustion, reactions can occur over a wide range of flow scales [2], and the use of the Kolmogorov mixing time scale could lead to inaccurate predictions of temperature and species mass fractions [25].

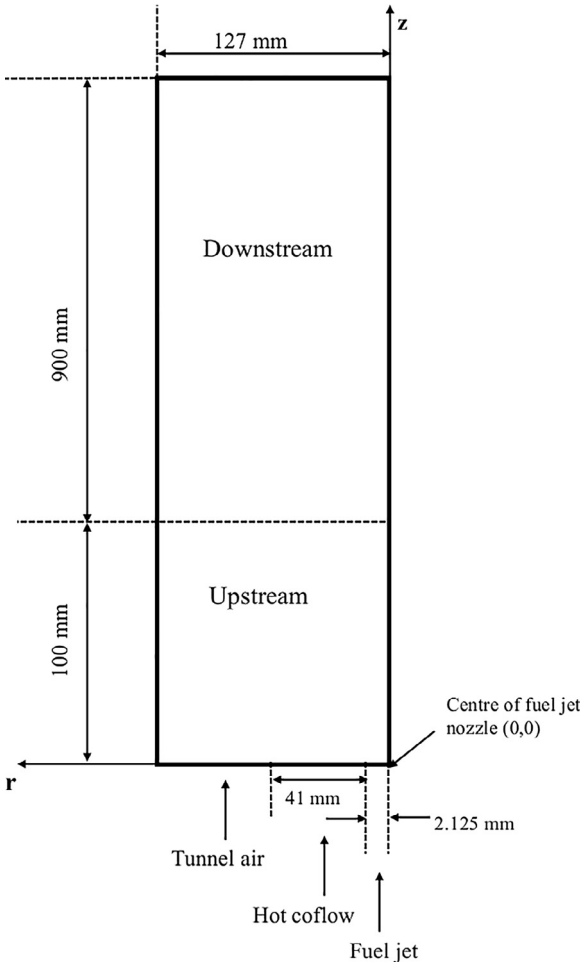

Fig. 2. 2D sketch of the Adelaide Jet in Hot Co-flow burner (adapted from Ferrarotti et al. [34]).

Table 2
Physical properties of the jet (Central jet velocity is for the Re = 10 k case.)

Profiles	Central jet	Annulus	Tunnel
Velocity	58.74 m/s	3.2 m/s	3.3 m/s
Temperature	294 K	1300 K	294 K

Integral time scale. Another characteristic time scale in turbulent flow is the eddy break-up time leading from large-scale to Kolmogorov-scale non-uniformities [17], which is also referred to as integral time scale, $\tau_{mix_I} = \frac{k}{\epsilon}$, where k is the turbulence kinetic energy.

Geometric mean of Kolmogorov and integral time scales. To provide a more accurate evaluation of the mixing time, Borghi [26] proposed to consider the whole spectrum of time scales. A simple approach to achieve this is to take only the two most important time scales, via the geometrical mean of the Kolmogorov and integral time scales [17], that

Table 3
Investigated cases.

Co-flow oxygen level:	3%	6%	9%
Re = 5000	✓		
Re = 10,000	✓	✓	✓
Re = 20,000	✓		

is:

$$\tau_{mix_{Mean}} = \sqrt{\tau_{mix_K}\tau_{mix_I}} = \sqrt{\frac{k}{\epsilon}\left(\frac{\nu}{\epsilon}\right)^{1/2}}. \quad (9)$$

Dynamic time scale. The three ways of estimating mixing scales introduced above can be regarded as global approaches. A more comprehensive approach consists in using a dynamic approach [27]. The dynamic estimation of mixing time scale is based on the ratio of the

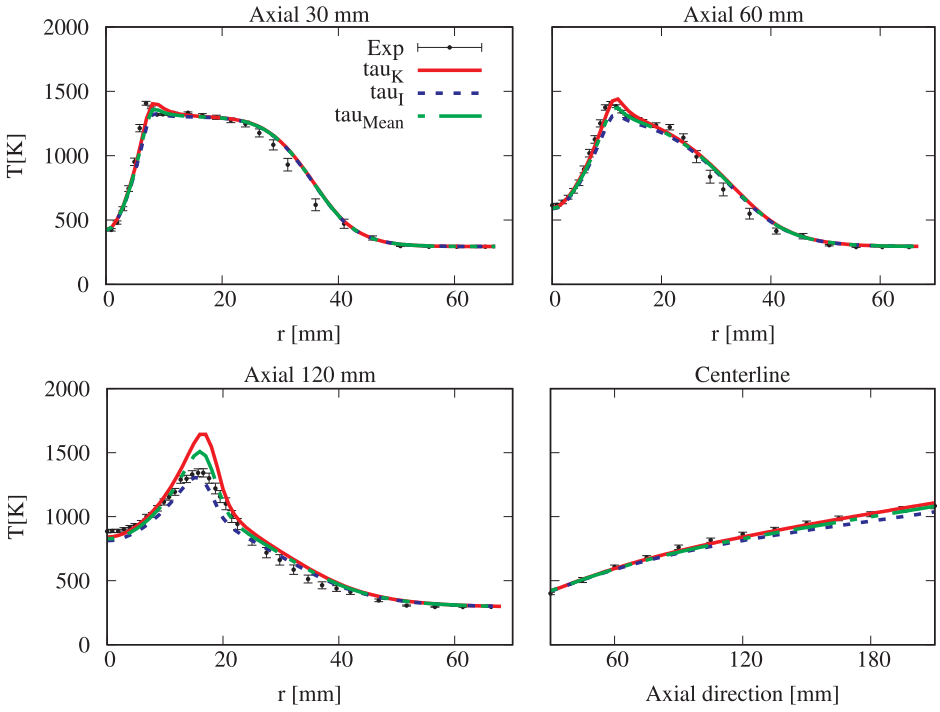

Fig. 3. Mean temperature profiles obtained with mixing time scale evaluated from the Kolmogorov scale (tau_K), the integral scale (tau_I) and the geometric mean of the two (tau_{Mean}).

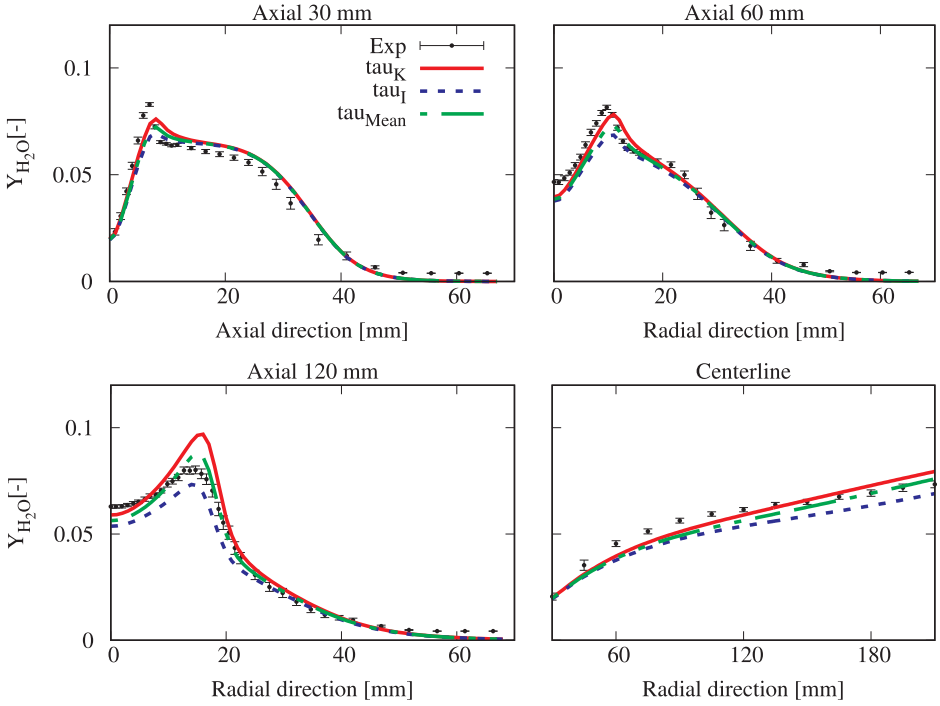

Fig. 4. Mean H_2O mass fraction profile obtained with mixing time scale evaluated from the Kolmogorov scale (tau_K), the integral scale (tau_I) and the geometric mean of the two (tau_{Mean}).

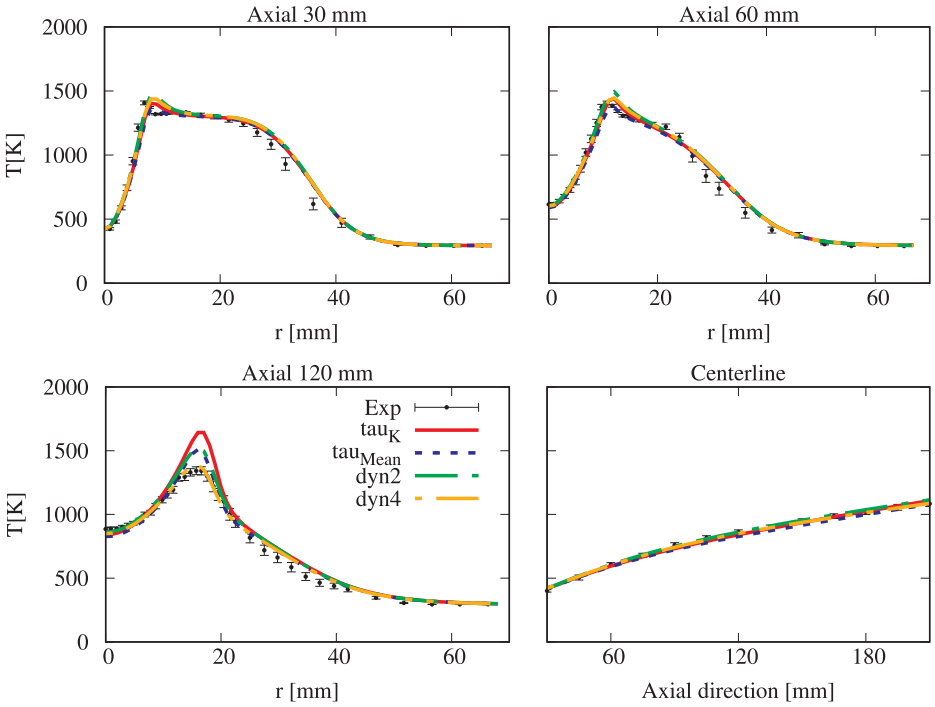

Fig. 5. Mean temperature profiles obtained with a mixing time scale evaluated using the Kolmogorov scale (tau_K), the geometric mean of Kolmogorov and integral scale (tau_{Mean}), the second (dyn2) and fourth (dyn4) parameter sets of the dynamic model.

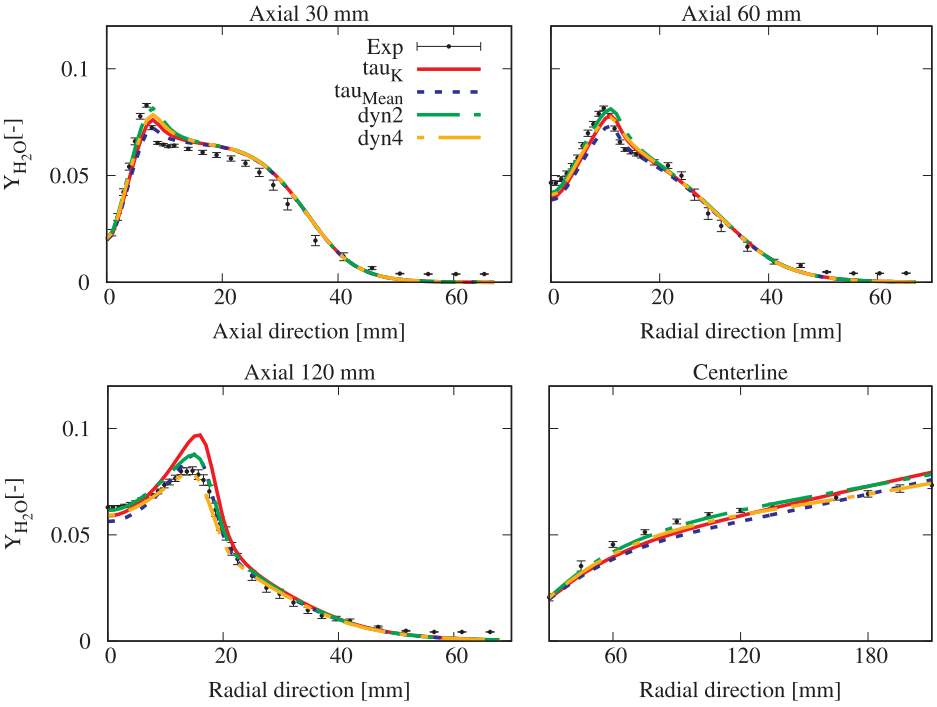

Fig. 6. Mean H_2O mass fraction profile obtained with mixing time scale evaluated from the Kolmogorov scale (tau_K), the geometric mean of Kolmogorov and integral scale (tau_{Mean}), the second (dyn2) and fourth (dyn4) parameter sets of the dynamic model.

scalar variance, $\widetilde{\phi''^2}$, to the scalar dissipation rate, $\widetilde{\epsilon}_\phi$ [28]:

$$\tau_{mix_{Dynamic}} = \frac{\widetilde{\phi''^2}}{\widetilde{\epsilon}_\phi}. \tag{10}$$

The mixture fraction f is selected to describe the mixing process of a scalar. Therefore, the scalar variance and dissipation rate take the form

Table 4
CPU time consumption of various mixing models.

Mixing model	Kolmogorov	Geometric mean	Dynamic	Integral
CPU time	1.0	1.4	1.53	1.85

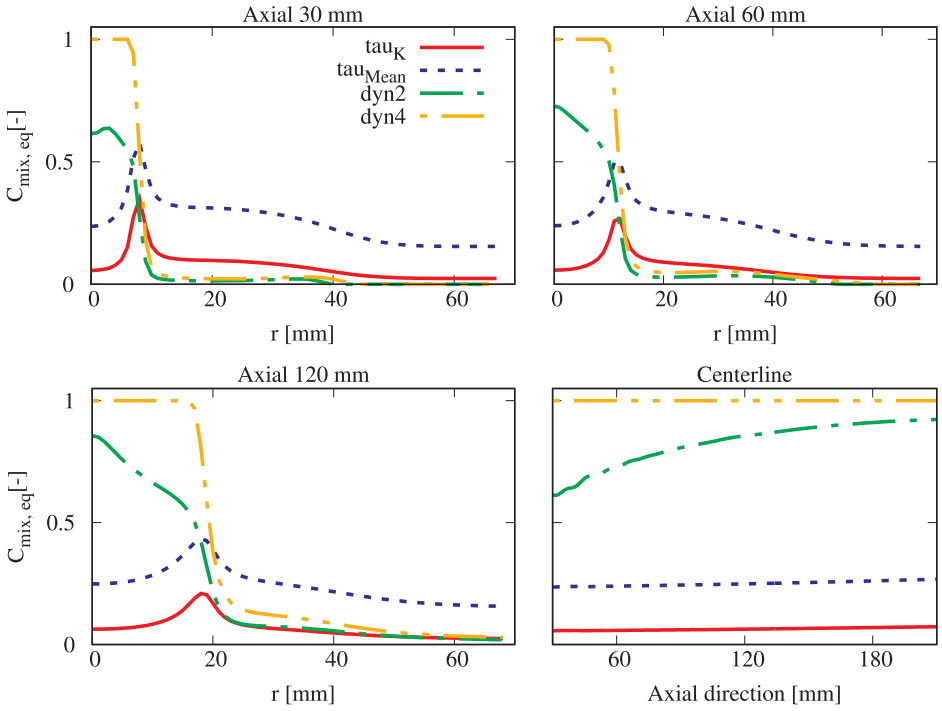

Fig. 7. $C_{mix,eq}$ profiles obtained with mixing time scale evaluated from using the Kolmogorov scale (tau_K), the geometric mean of Kolmogorov and integral scale (tau_{Mean}), the second (dyn2) and fourth (dyn4) parameter sets of the dynamic model.

of the mixture fraction variance ($\widetilde{f''^2}$) and mixture fraction dissipation rate ($\widetilde{\chi}$). They are modelled with the following transport equations [29,30]:

$$\frac{\partial \overline{\rho}\widetilde{f}}{\partial t} + \frac{\partial \overline{\rho}\widetilde{u_j}\widetilde{f}}{\partial x_j} = \frac{\partial}{\partial x_j}\left(\rho(D+D_t)\frac{\partial \widetilde{f}}{\partial x_j}\right), \tag{11}$$

$$\frac{\partial \overline{\rho}\,\widetilde{f''^2}}{\partial t} + \frac{\partial \overline{\rho}\widetilde{u_j}\,\widetilde{f''^2}}{\partial x_j} = \frac{\partial}{\partial x_j}\left(\rho(D+D_t)\frac{\partial \widetilde{f''^2}}{\partial x_j}\right) + 2\rho D_t\left(\frac{\partial \widetilde{f}}{\partial x_j}\right)^2 - \overline{\rho}\widetilde{\chi}, \tag{12}$$

$$\frac{\partial \overline{\rho}\widetilde{\chi}}{\partial t} + \frac{\partial \rho\widetilde{u_j}\widetilde{\chi}}{\partial x_j} = \frac{\partial}{\partial x_j}\left(\rho(D+D_t)\frac{\partial \widetilde{\chi}}{\partial x_j}\right) - C_1\overline{\rho}\frac{\widetilde{\chi}^2}{\widetilde{f''^2}} - C_2\overline{\rho}^2\frac{C_\mu\widetilde{k}}{\mu_t}\widetilde{\chi} + C_3\frac{\overline{\rho}C_\mu\widetilde{k}}{Sc_t}\left(\frac{\partial \widetilde{f}}{\partial x_j}\right)^2 + C_4\mu_t\frac{\widetilde{\chi}}{\widetilde{k}}|\widetilde{S}|^2. \tag{13}$$

In Eq. (13), C_1,C_2,C_3 and C_4 are model constants. Four different set of values were proposed in [29], as shown in Table 1. Based on a sensitivity study, the present work focuses on the results obtained with set 2 and set 4.

2.4. Chemical time scale evaluation in PaSR

Chemical time scale estimation from Jacobian matrix eigenvalues. For the evaluation of chemical time scale, Fox [31,32] suggested using the eigenvalues of the Jacobian matrix **J** of the chemical source terms. The Jacobian matrix **J** has the dimension of $i \times i$, where i is the number of chemical species in the mechanism. Each element J_{jk} of the matrix is expressed as:

$$J_{jk} = \frac{\partial R_j^*}{\partial Y_k^*}, \tag{14}$$

where the superscript $*$ denotes reactive structures values. After the decomposition of the Jacobian matrix, the chemical time scale is estimated with the inverse of the eigenvalues λ_i:

$$\tau_{c,i} = \frac{1}{|\lambda_i|}. \tag{15}$$

In Eq. (15), $\tau_{c,i}$ is the characteristic time scale of a single species. After removing the dormant species (characterised by infinite time scale values), the slowest chemical time scale is chosen as leading scale for the evaluation of the PaSR parameter κ.

Chemical time scale estimation from formation rates. The decomposition of the source term Jacobian matrix is accurate but time consuming, especially when large scale simulations with much detailed mechanism is used. The formation rate based characteristic time scale evaluation is a simplified approach. Instead of getting the chemical time scale for each species from the Jacobian matrix decomposition, the ratio of species mass fraction and formation rate in the reactive structure is directly used [17,33], approximating the Jacobian diagonal terms:

$$\tau_{c,i} = \frac{Y_i^*}{|dY_i^*/dt|}. \tag{16}$$

Chemical time scale estimation from reaction rates. Another simplified method is based on the reaction rate. Similar to the two approaches above, the characteristic time scale for each species i is expressed as [18]:

$$\tau_{c,i} = \frac{n_r \cdot cTot^*}{\sum_{n=1}^{n_r}\left((dc^*_{n_r,forward}/dt)\cdot\nu_{n_r,sum}\right)}, \tag{17}$$

where n_r is the number of reactions, and $cTot^*$ is the total concentration obtained from the ideal gas law. Only the forward reaction rate $dc^*_{n_r,forward}/dt$ is used here. The term $\nu_{n_r,sum}$ represents the sum of the product stoichiometric coefficients.

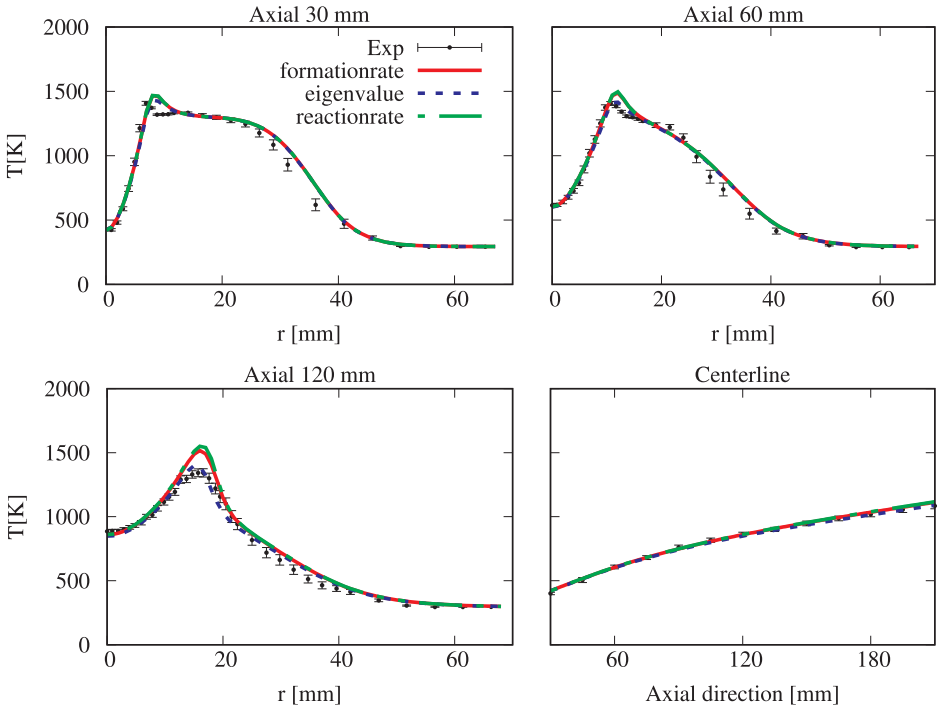

Fig. 8. Mean temperature profiles obtained with chemical time scale evaluated from the formation rates, the Jacobian eigenvalues and the reaction rates.

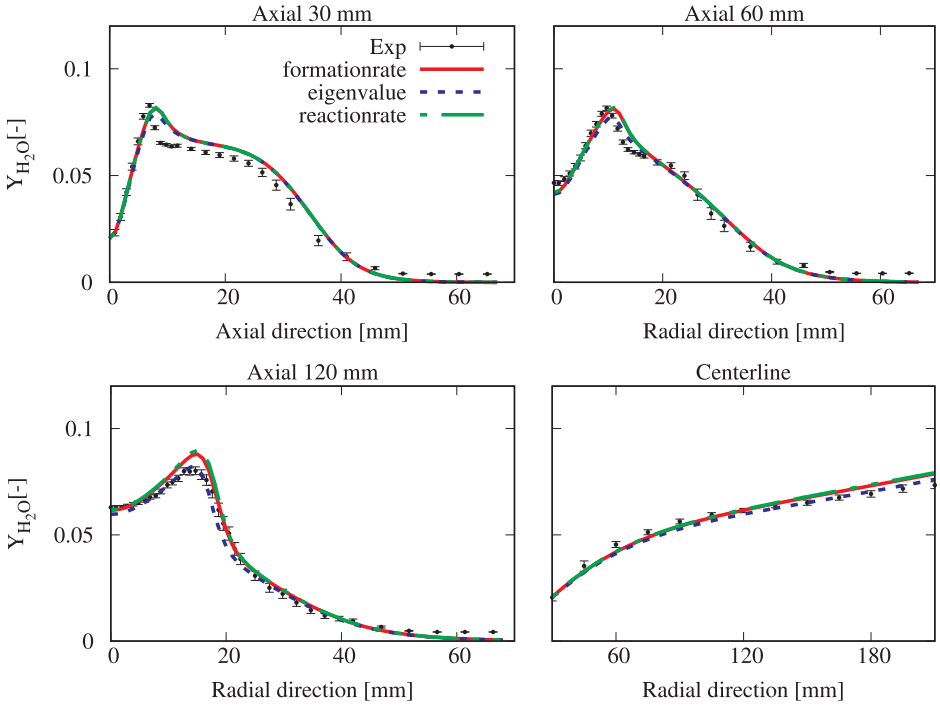

Fig. 9. Mean H_2O mass fraction profiles obtained with chemical time scale evaluated from the formation rates, the Jacobian eigenvalues and the reaction rates.

3. Model validation

3.1. Experimental data

The AJHC burner emulates MILD combustion with a simple geometry. It has an insulated and cooled central jet with the inner diameter of 4.2 mm, providing an equi-molar mixture of CH_4 and H_2. There is an annulus pipe with a secondary burner mounted upstream. The burner provides hot combustion products, which are further mixed with air and nitrogen in order to control the oxygen levels to 3%, 6% and 9% in mass fraction. The annulus inner diameter is 82 mm. The wind tunnel, on which the burner is mounted, has the cross section of

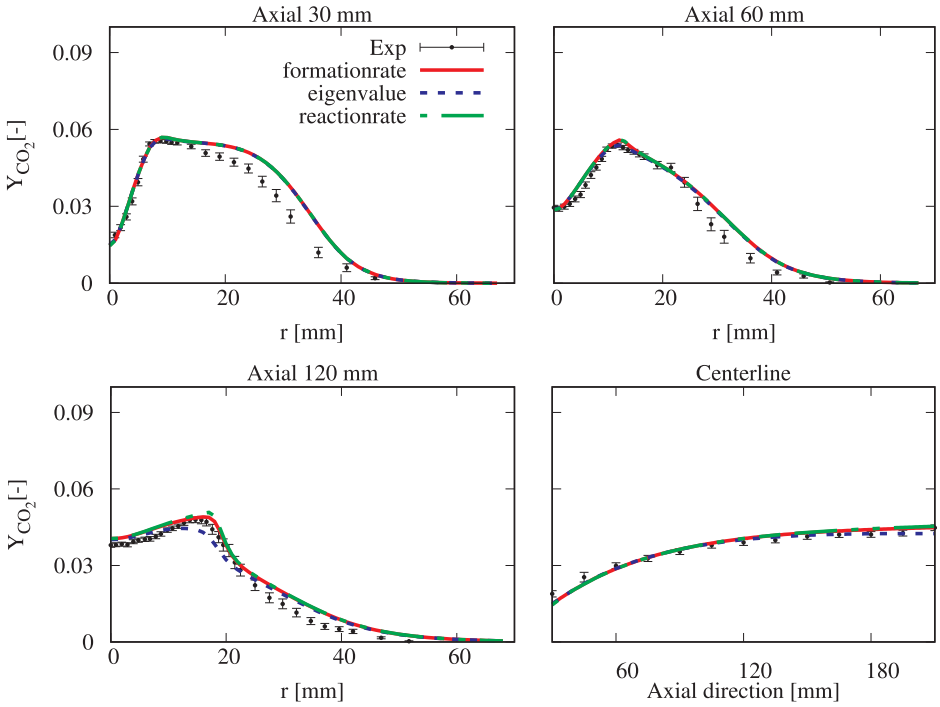

Fig. 10. Mean CO_2 mass fraction profiles obtained with chemical time scale evaluated from the formation rates, the Jacobian eigenvalues and the reaction rates.

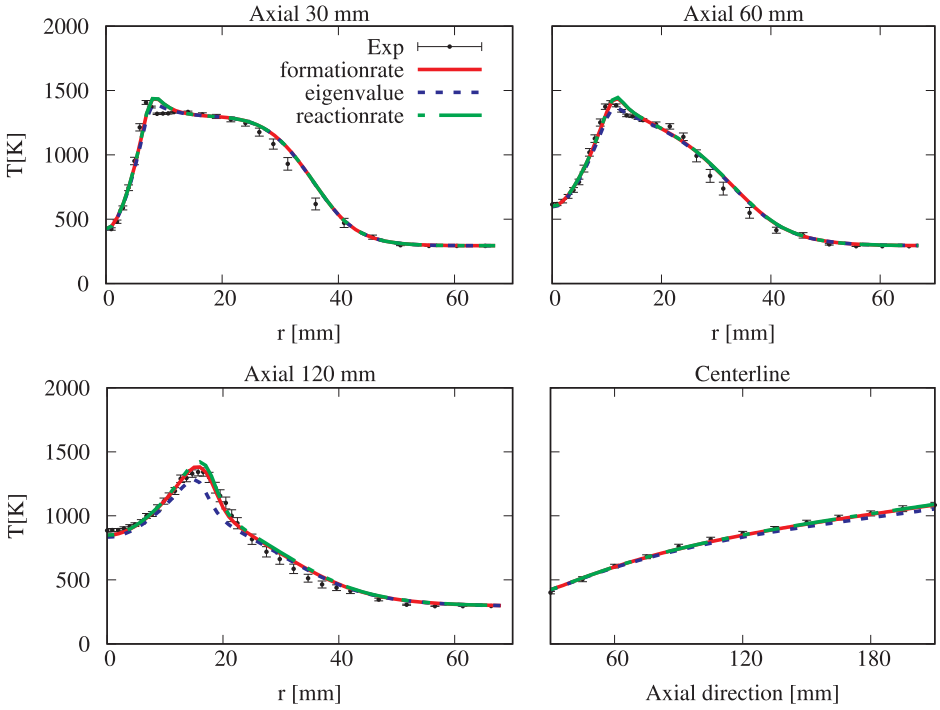

Fig. 11. Mean temperature profiles obtained with chemical time scale evaluated from the formation rates, the Jacobian eigenvalues and the reaction rates. With dyn4 model.

254 mm × 254 mm. In Fig. 2, a 2D simple sketch of the investigated area in the numerical modelling is presented. The central jet, annulus and wind tunnel gas temperatures and velocities (for the Re = 10 k case) are presented in Table 2. In the current study, 5 cases with the combination of different co-flow oxygen contents and fuel jet Reynolds numbers are investigated, as highlighted in Table 3. The other conditions are not investigated since no experimental data are provided for them.

The mean, variance and scattered data of temperature and various

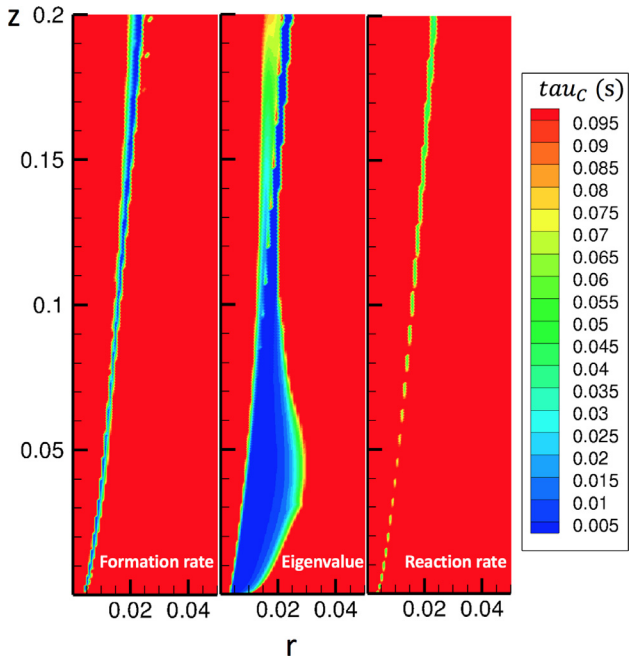

Fig. 12. Chemical time scale (tau_C) distribution estimated from the formation rates, the Jacobian eigenvalues and the reaction rates. Only the area of interest of the simulation domain is shown. Legend unit: m. OpenFOAM solver.

species mass fractions (CH_4, H_2, H_2O, CO_2, N_2, O_2, NO, CO, and OH), along the centerline as well as on the different axial locations of 30/60/120/200 mm (z = 30/60/120/200 mm), are available for validation. The experimental profiles used for comparison include both the mean values and the error bar with 99.99% confidence interval associated with a Student's distribution for the true mean value [35].

3.2. Numerical set-up

Based on a Grid Convergence Index (GCI) study [33], a 2-dimensional structured axis-symmetric mesh with ~31,500 cells was used in the simulations. The computational domain starts from the burner exit and extends 1000 mm further downstream. Second order discretization schemes for space and time are applied. Both non-uniform and uniform boundary conditions are used in the simulation for the species mass fractions and temperature. The non-uniform boundary conditions are based on the profiles of O_2, CO, CO_2, H_2O mass fractions and temperature, obtained from the experimental data at 4 mm downstream of the burner exit. The uniform boundary conditions are set according to Dally et al. [22]. Additional details about the numerical settings can be found in [33].

Unsteady simulations were carried out using two solvers, the PaSRPimpleSMOKE [24,36] solver, based on OpenFOAM®, and ANSYS Fluent 17.0 unsteady solver. The PaSR model and different formulations of mixing and chemical time scale estimation were implemented in ANSYS Fluent 17.0 via a bespoke user-defined function. Multi-component molecular diffusion was included, because of the presence of hydrogen in the fuel. Since preliminary simulations with ANSYS Fluent 17.0 showed (see supplementary material 5) that radiation does not impact significantly the temperature and species profiles at the locations of interest, it was not included in the present study. A reduced skeletal mechanism KEE58 [37], with 17 species and 58 reactions, was chosen for finite rate chemistry approach. The turbulent Schmidt and Prandtl numbers are set to 0.7 and 0.85, respectively. Previous work on the AJHC burner ([38,39]) showed improved prediction with the modified $C_{1\epsilon}$ constant in the standard $k-\epsilon$ model. In the current study, the $C_{1\epsilon}$ constant was increased from 1.44 to 1.60 [40], to correct the well-known round-jet anomaly.

4. Results and discussion

In this section, the influence of different choices of mixing and chemical time scales in the context of the PaSR model is shown. The case corresponding to 3% O_2 in the co-flow and Re = 10,000 is used for validation in Sections 4.1 and 4.2. In Section 4.3, the influence of co-flow oxygen levels (6% and 9%) and Reynolds numbers (Re = 5000 and Re = 20,000) is shown. Modelling results obtained with OpenFOAM and ANSYS Fluent 17.0 are benchmarked, for all the five cases in Table 3. In Section 4.4, the effect of specifying non-uniform boundary conditions for the thermo-chemical scalars is discussed, with special focus on CO prediction.

4.1. Influence of mixing time scale estimation

The mean temperature profiles obtained with mixing time scale estimated with the Kolmogorov scale, the integral scale and the geometric mean of the two are compared and validated against experimental data in Fig. 3 at several sampling locations. The chemical time scale is estimated from the formation rates and uniform boundary conditions are used.

Fig. 3 shows that the use of a mixing scale based on the Kolmogorov one results in temperature over-prediction at z = 60 mm and, more significantly, at z = 120 mm. Using the integral mixing time scale, the temperature profiles are under-predicted at z = 30 mm and 60 mm downstream of the burner exit, and along the centerline. On the other hand, the temperature peak at 120 mm axial location is well predicted. However, the use of the integral mixing time scale strongly under-predicts the H_2O profile at 120 mm axial location, as indicated in Fig. 4. When the geometric mean of the two scales is used, the z = 30 mm/60 mm and centerline temperature profiles agree well with the experimental ones. A slight over-prediction of the temperature profile at 120 mm can be observed. However, the H_2O mass fraction profiles at z = 30 mm and 60 mm are significantly under-predicted. The use of the Kolmogorov mixing time scale improves H_2O prediction upstream ($z \leqslant 00$ mm).

From the results above, one can conclude that the global defined mixing time scale is not suitable for the whole flow field condition. The use of a dynamic mixing model potentially offers a solution to this, by providing locally an optimal mixing scale. The dynamic model is compared with the global approaches in Fig. 5. No major differences can be observed at z = 30 mm/60 mm and along the centerline for the temperature value. At 120 mm axial location, the temperature over-prediction is corrected using the dynamic model with coefficient set 4 (Table 1), indicated as dyn4 in short. The same can be observed for the H_2O mass fraction profiles in Fig. 6, whose prediction is strongly improved using the dyn4 model. At z = 30 mm, better prediction of the H_2O peak value using the dyn2 model can be also observed.

The scaled CPU time associated to the various mixing models are estimated taking the Kolmogorov mixing scale as reference in Table 4. Even though using the kolmogorov time scale reduces the CPU time, this would lead to non-negligible over-prediction of mean temperature and species mass fraction at z = 120 mm (see Figs. 3 and 4). On the other hand, the dynamic model requires medium CPU time, while

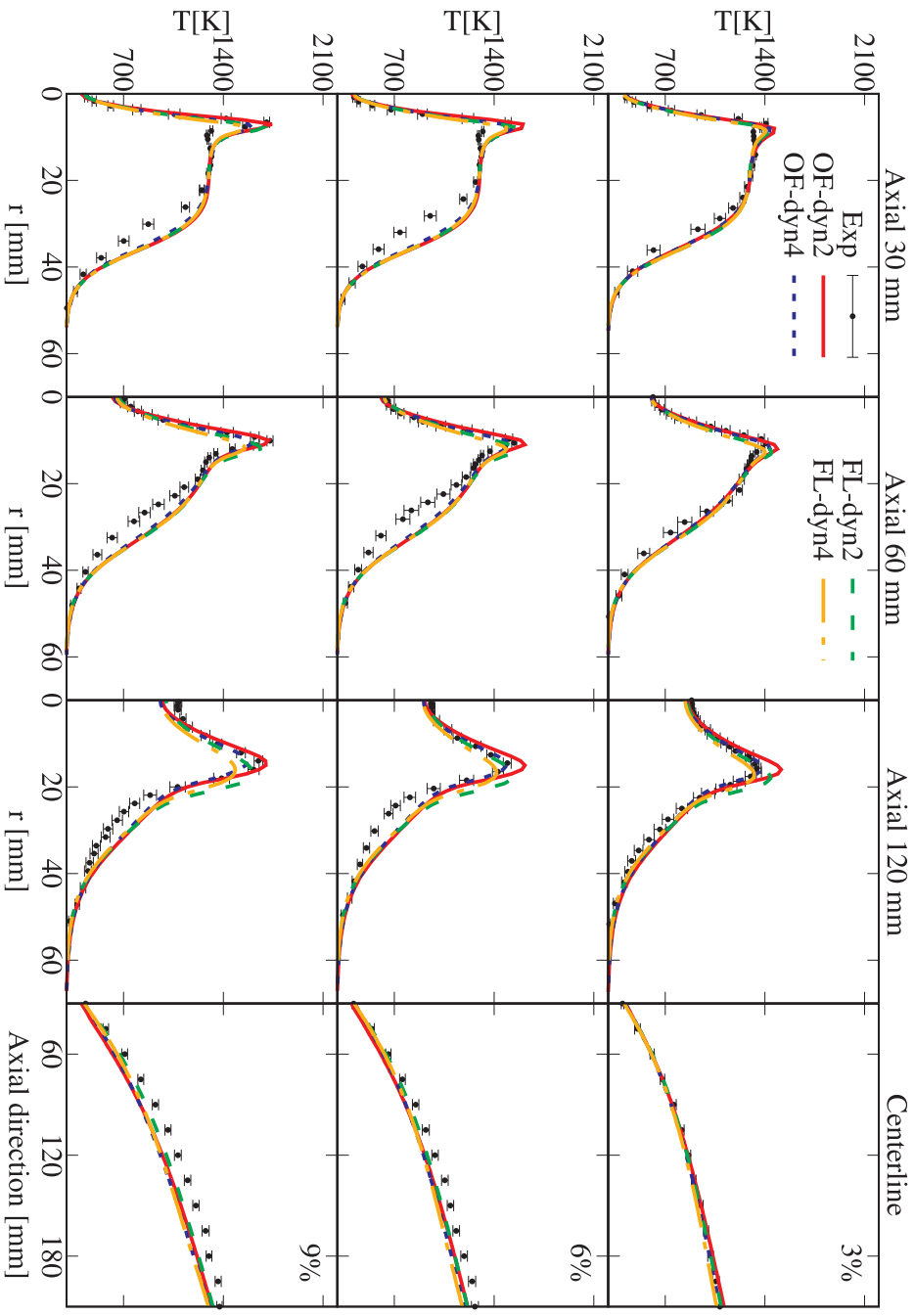

Fig. 13. Mean temperature profiles obtained for different co-flow oxygen levels (3%, 6% and 9%), using two dynamic model formulations. OpenFOAM and Fluent solvers.

showing superior results compared to all the other models.

To summarize, the use of a dynamic model (especially dyn4) can correctly fix the temperature over-prediction at 120 mm, without compromising the predictions at z = 30 mm and 60 mm (see the integral mixing scale profiles in Fig. 3). Furthermore, the dynamic model reproduces the species mass fraction profiles accurately, which is not the case with the globally defined time scales.

To highlight the differences between the global and dynamic scale definition, an equivalent C_{mix} value is defined as $C_{mix,eq} = \tau_{mix}/\tau_I$, where τ_{mix} is the mixing scale provided by the different approaches, i.e. global and dynamic. The equivalent C_{mix} values at several locations of interest are shown in Fig. 7. A first observation is that $C_{mix,eq}$ is bounded smaller than 1, indicating a time scale ranging from the Kolmogorov to the integral one. Looking at the radial profiles, there is a location where the $C_{mix,eq}$ profiles associated to the Kolmogorov (red[1] solid line) and dyn2 (green dashed-dotted line) mixing scale models intersect. The same happens for the profiles provided by the geometric mean (blue dotted line) and dyn4 (orange dotted-dashed line) models, at almost the same location. The intersection occurs at radial locations of 7–8 mm, 11–12 mm and 19–20 mm for z = 30/60/120 mm positions, respectively. They are adjacent to the locations of maximum temperatures, i.e. 6.9 mm, 10.7 mm and 16.6 mm for z = 30/60/120 mm, respectively. All the mixing models in Fig. 7 are able to capture the interaction between the fuel and co-flow streams, but only the dynamic ones can

[1] For interpretation of color in Figs. 7 and 16, the reader is referred to the web version of this article.

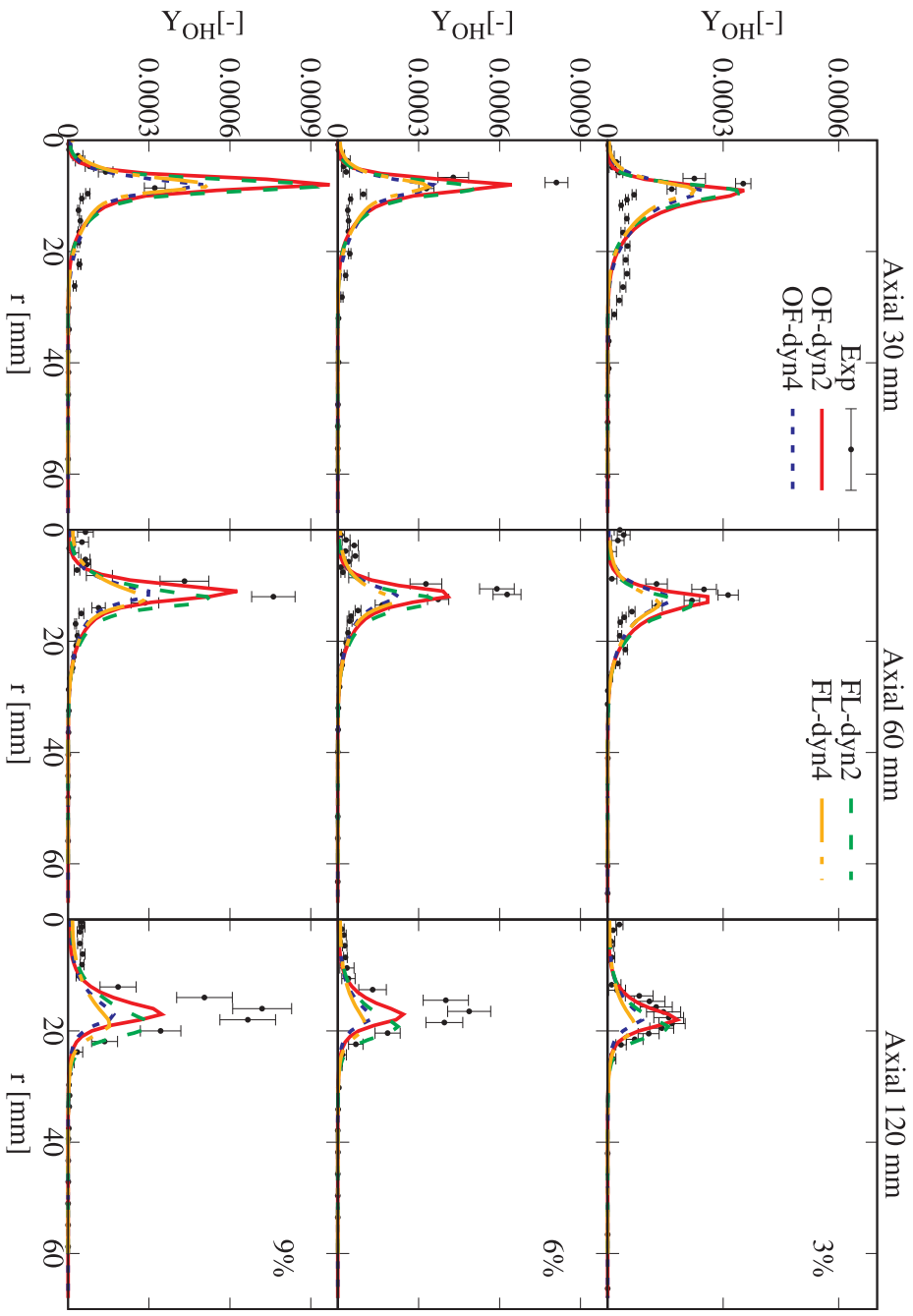

Fig. 14. Mean OH mass fraction profile obtained for different co-flow oxygen levels (3%, 6% and 9%), using two dynamic model formulations. OpenFOAM and Fluent solvers.

account for the breakup of large eddies into smaller ones downstream of the jet, providing $C_{mix,eq}$ values decreasing from 1.0 to lower values. Among the dynamic model variants, the dyn4 always provides higher $C_{mix,eq}$ values, corresponding to lower κ in PaSR model. The effect of the different $C_{mix,eq}$ values provided by the two dynamic models can be appreciated from the mean temperature and H_2O profiles in Figs. 5 and 6.

4.2. Influence of chemical time scale estimation

From Section 4.1, the dynamic mixing model has proven to be more superior to other approaches for mixing time scale evaluation and it is then set as a default for further investigation. Fig. 8 shows the mean temperature profiles adopting different approaches to estimate the chemical time scales. The dyn2 mixing model is used and uniform boundary conditions are applied. As observed in Fig. 8, the

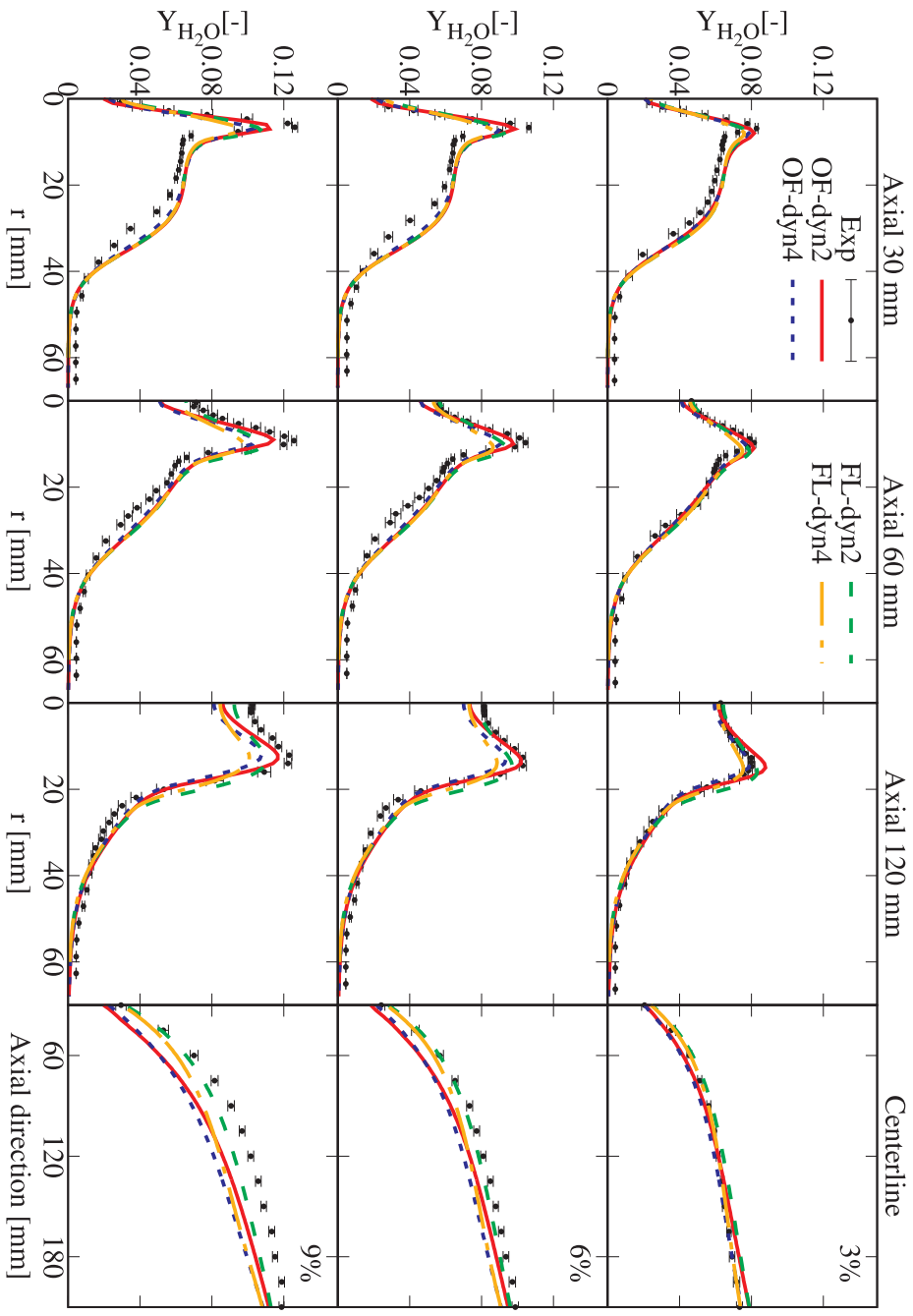

Fig. 15. Mean H_2O mass fraction profile obtained for different co-flow oxygen levels (3%, 6% and 9%), using two dynamic model formulations. OpenFOAM and Fluent solvers.

dyn2 mixing model, in combination with the chemical time scale calculation based on the formation rate, over-predicts the mean temperatures. This is especially obvious at z = 120 mm, where the peak temperature is over-predicted by 123 K. The evaluation of the chemical time scale using the reaction rate based approach provides very similar results, with a temperature over-prediction at z = 120 mm of 172 K. On the other hand, estimating the time scale from the formation rate Jacobian, the mean temperature is correctly predicted, at all axial locations.

As far as species predictions are concerned, the H_2O mass fraction profiles are shown in Fig. 9. It can be observed that the approaches based on the formation and reaction rates provide more accurate predictions upstream, while using the Jacobian eigenvalues improves the predictions downstream. At z = 120 mm, the use of formation and reaction rates for chemical time scale evaluation lead to over-prediction errors of 7% and 9.2%, respectively. As for CO_2 (Fig. 10), the

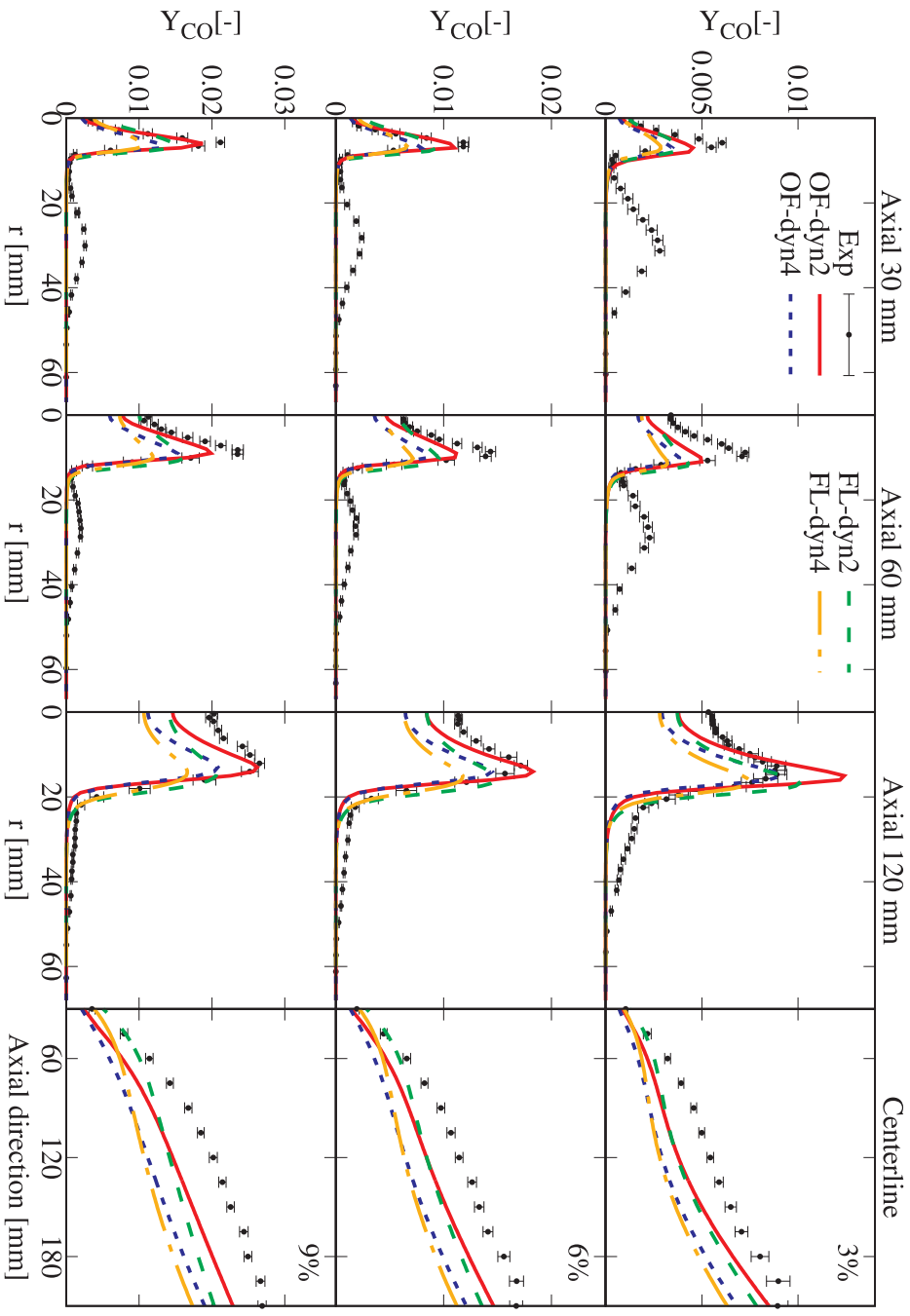

Fig. 16. Mean CO mass fraction profile obtained for different co-flow oxygen levels (3%, 6% and 9%), using two dynamic model formulations. OpenFOAM and Fluent solvers.

eigenvalue approach slightly under-predicts the peak value (by 4.8%) at axial 120 mm, while the reaction rate approach over-predicts it by about 4%.

The results obtained using the dyn4 model are also shown in Fig. 11. Being different from Fig. 8, the various approaches used for the evaluation of the chemical time scale predict the mean temperatures accurately. This is expected, considering that the dyn4 model predicts larger C_{mix} and, thus, larger τ_{mix} values, making the PaSR approach less dependent on the chemical time scale (see the definition of κ in Eq. (6)).

Fig. 12 shows contour plots of the local chemical time scales estimated with the three methods. The eigenvalue-based approach shows

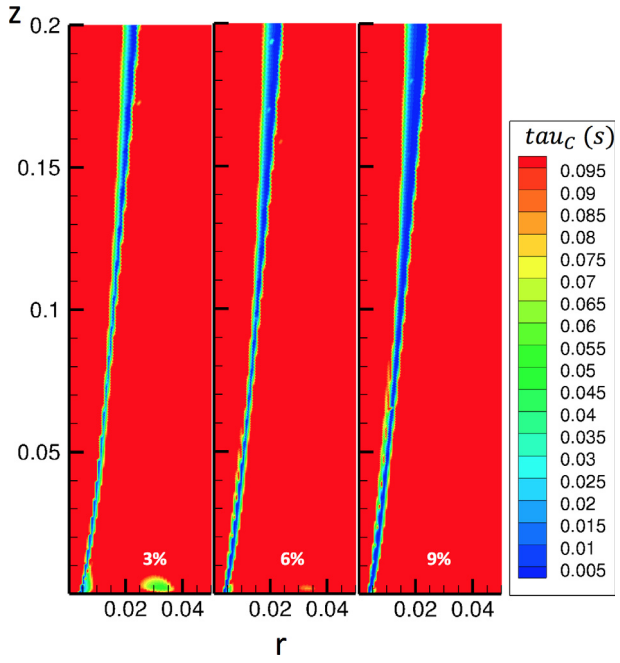

Fig. 17. Chemical time scale (tau_C) distribution. Mixing time scale estimated from the dyn2 mixing model. Only the area of interest of the simulation domain is shown. Legend unit: m. OpenFOAM solver.

wider reaction region (the blue area with $tau_C \leqslant 0.02$ s), whereas the other two models estimate these regions to be dormant and set $tau_C = 0.1$ s, which is the maximum cut-off value for the chemical time scale. Comparing the formation and reaction rate based methods, the latter gives higher tau_C values in the combustion region, which implies higher κ, leading to the observed over-prediction of mean temperature and specie mass fractions, especially at downstream locations. In summary, the chemical time scale evaluation from reaction rates tends to over-estimate the κ values in the PaSR approach, while the formation rate and eigenvalue methods correct this, improving the thermo-chemical scalar predictions.

4.3. Comparison with Fluent

The present section shows a throughout comparison between the OpenFOAM and ANSYS Fluent solvers, for the different cases in Table 3. Second-order temporal and spatial discretizations schemes are used for both OpenFOAM and ANSYS Fluent. Both solvers adopt the PIMPLE algorithm for a URANS simulation. Chemical and mixing time scales are evaluated using the formation rate based and dynamic model, respectively. Results from both the second and fourth sets of dynamic mixing time scale evaluation model parameters are shown. Uniform boundary conditions are used. The mean temperature profiles are first presented in Fig. 13. The 10,000 Reynolds number case is considered, adjusting the oxygen content in the co-flow to 3%, 6% and 9%. The abbreviation OF means that the data are obtained from OpenFOAM simulation, while FL denotes ANSYS Fluent.

Both solvers are able to provide satisfactory predictions of mean temperatures, at different oxygen levels. Similarly to OF, the FL results obtained with the dyn2 model show higher temperature levels when compared to the dyn4 model. The dyn4 model provides better predictions with both solvers, for a co-flow oxygen level equal to 3%, especially at z = 120 mm. For 6% and 9% O_2 levels, the FL results with dyn4 cannot predict the peak temperature accurately, and the dyn2 model is found to perform better. The same is found using OpenFOAM. In general, FL results present slightly lower temperature values with respect to OF, and it provides radially shifted temperature peaks. The observed differences could be caused by the more dissipative nature of FL with respect to OF, as documented in [41]. The same conclusion can be drawn from the species mass fraction profiles in Figs. 14–16.

Capturing the OH radical mass fraction distribution is very important, as it can be used as flame marker. In Fig. 14, the experimental and numerical profiles of OH mass fraction are shown, for different O_2 levels in the co-flow (3%, 6% and 9%). The results obtained with both solvers are very close to each other. The dyn2 mixing model shows excellent agreement with the experimental data for 3% co-flow O_2 level, while slight under-predictions are observed for 6% and 9%, at z = 60 mm and 120 mm. A more pronounced over-prediction of the OH peak can be detected at 30 mm axial location, for the 9% O_2 case. On the other hand, the FL and OF results obtained with dyn4 mixing model are able to reproduce the experimental peak values with satisfactory accuracy.

The analysis of the H_2O profiles in Fig. 15 reveals interesting information. Overall, satisfactory predictions of H_2O mass fraction profiles is obtained with both OF and FL, for the case of 3% O_2. For the 6% and 9% O_2 case, the centerline measurements are significantly under-predicted with OF solver, particularly at upstream locations. The under-prediction along the centerline could be detected, although less significant, also for the temperature profile in Fig. 13. As for the CO_2 mass fraction profiles (not-shown here), no under-prediction exists for upstream centerline values. Therefore, it can be concluded that the temperature under-prediction observed for the 6% and 9% O_2 cases, is associated to the under-prediction of H_2O production, which affects the heat release rate and the temperature levels. The FL solver with dyn2 model, however, provides better prediction on the centerline results for 6% and 9% O_2 cases. As far as the radial species profiles are concerned, the OF results with the dyn2 model show the highest accuracy, whereas all other combinations show obvious under-prediction, especially for the peak values. The FL solver shows in general a bit lower predicted profile than that with OF solver. A slightly shifted peak values can also be captured. The OF solver with the dyn2 mixing model provides the best predictions of the CO mass fraction profiles, as indicated in Fig. 16 by the red solid line. The CO profiles for 3% O_2 and z = 120 mm are slightly over-predicted by the dyn2 model, while the OF results with dyn4 and FL with dyn2 provide better results. All solver and dynamic model combinations cannot accurately reproduce the centerline profile.

The analysis of the CO radial profiles in Fig. 16 shows the existence of a second peak, at $z \leqslant 60$ mm, in the measurement data. This is due to the non-zero CO concentration in the hot co-flow, that is convected downstream. Because uniform boundary conditions are adopted in the simulations, this second peak can not be captured. A discussion about the influence of boundary conditions on the prediction of CO is presented in Section 4.4.

The results shown above refer to cases with a fixed Reynolds number, varying the O_2 content in the co-flow. This means that the mixing time is not strongly affected, while the chemical time scale changes due to the change of the oxidizing atmosphere. The contour plots showing the chemical time scale distributions for the three O_2

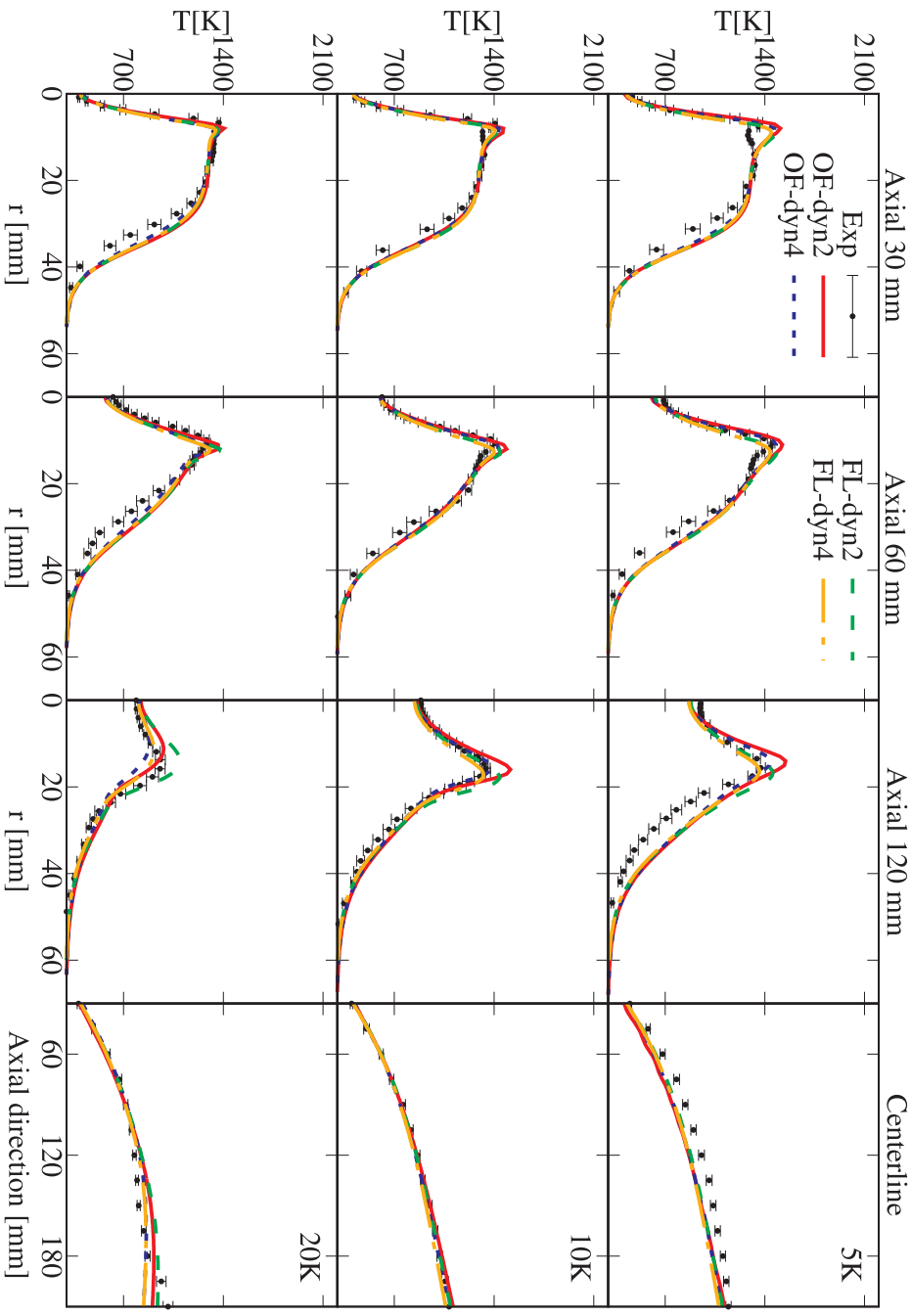

Fig. 18. Mean temperature profiles obtained for different fuel jet Reynolds numbers (5 k, 10 k and 20 k), using two dynamic model formulations. OpenFOAM and Fluent solvers.

level cases (3%, 6% and 9%) are compared in Fig. 17. With increasing oxygen content, more oxygen is available to mix with the fuel stream, and the reaction process is enhanced. This can be well indicated by the expansion of the reactive region in the flow, which is characterized by chemical time scales (tau_C) smaller than the fixed threshold value of 0.1 s.

For the purpose of investigating how the model performs for varied flow field, cases with different fuel jet Reynolds numbers are simulated, fixing co-flow oxygen content to 3%. The mean temperature profiles and distribution of $C_{mix,eq}$ values are presented in Figs. 18 and 19, separately. The mean temperature profiles are mostly well predicted with both solvers and parameter sets. The dyn2 model with OpenFOAM solver gives some over-predictions at z = 120 mm. While the dyn2 model with FL solver alleviates the over-prediction, except for the case

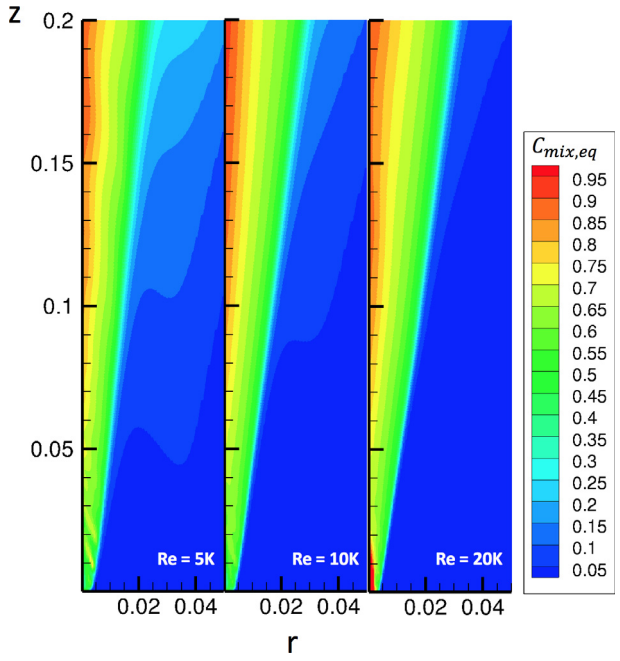

Fig. 19. Mixing time constant C_{mix} distribution for the different fuel jet Reynolds number cases (5 k, 10 k and 20 k). Only the area of interest of the simulation domain is shown. Legend unit: m. OpenFOAM solver.

of $Re = 20$ k. As for the $Re = 20$ k at 120 mm axial location, the dyn2 model with OpenFOAM solver gives overall more satisfactory prediction. On the other hand, the FL solver with the dyn2 model shows non-negligible over-prediction of temperature levels. Moreover, both dyn2 and dyn4 models with the FL solver show flame extinction for the 20 k case above $z \geqslant 150$ mm.

The $C_{mix,eq}$ distribution with various fuel jet Reynolds numbers can be appreciated in Fig. 19. The $Re = 5$ k case shows a pronounced shear layer between the co-flow and fuel jet. This layer is progressively reduced when increasing the Reynolds number to 10 k and 20 k. The reason is that the increased fuel jet velocity reduces the inter-facial area and diminishes mixing [42]. Furthermore, for $Re = 20$ k, there is a high $C_{mix,eq}$ region in the jet potential core and further downstream, the $C_{mix,eq}$ value close to centerline is increased with increased Reynolds number. For a fully developed turbulent pipe flow, the turbulent intensity has a negative correlation with the Reynolds number, meaning that higher Reynolds number jet breaks up later than the one with lower Reynolds number [43,44]. Therefore, a larger mixing scale is found for the case with higher Reynolds number, thus resulting in higher τ_{mix} value and lower values of reacting fractions. This justifies the reduction of the temperature levels going from Re = 5 k to Re = 20 k, as seen in Fig. 18.

4.4. Influence of boundary conditions on CO prediction

The CO mass fraction profiles obtained with non-uniform and uniform boundary conditions are presented in Figs. 20 and 21. The mixing model dyn2 is used and the chemical time scale is calculated with the formation rate based approach. It is very clear that the use of non-uniform boundary conditions helps to improve the CO predictions, as it allows capturing the second radial peak, without impairing the prediction of the first peak for 6% and 9% O_2 cases in Fig. 20. On the other hand, the use of non-uniform boundary conditions worsen the CO prediction at z = 30 mm and z = 60 mm, for the 3% O_2 case, and for all O_2 levels along the centerline. Regarding the temperature profile (not-shown here), using non-uniform boundary conditions corrects the temperature peak over-prediction by the dyn2 model, while the centerline value is under-estimated.

Fig. 21 shows the mean CO profiles obtained using the uniform and non-uniform boundary conditions, when varying the fuel jet Reynolds number. It can be observed that using the non-uniform boundary conditions allows capturing the second CO peak, but it significantly impacts the accuracy in the reconstruction of the first peak. Moreover, the use of non-uniform boundary conditions leads to the global extinction of the flame for the case of $Re = 20$ k, after z = 120 mm (from the burner exit).

5. Conclusion

In the current article, different approaches for mixing time scale and chemical time scale estimation are assessed and benchmarked, for their use in the context of the Partially-Stirred Reactor closure. The OpenFOAM and ANSYS Fluent 17.0 [21] solvers are compared on a variety of cases, varying the oxygen content in the co-flow and the fuel jet Reynolds number. The influence of using non-uniform and uniform boundary conditions is also assessed. The following conclusions can be drawn:

- The dynamic mixing model can identify optimal local values of the mixing time scale when compared to global approaches based on the Kolmogorov and integral scales, or combination of the two. The mean temperature profile on axial 120 mm location is well predicted using a dynamic mixing model without compromising the prediction at z = 30 mm. Therefore, the appropriate mixing scale was found to improve the prediction of the temperature and species profiles (especially H_2O) in the whole domain significantly, and it is not only in specific regions, as reported in the literature with other ad hoc approaches.
- The decomposition of the source term Jacobian matrix is the most accurate and time consuming method for the evaluation of the chemical time scale. The approach based on the formation rates provides the best compromise between accuracy and computational cost, while the approach based on reaction rates may lead to inaccurate results as it tends to over-predict the chemical time scales.
- The combination of the dynamic mixing model and the formation rate based chemical time scale estimation approach performs the best for applications under Moderate or Intense Low oxygen Dilution combustion condition, with a wide range of oxygen levels (3%, 6% and 9%) in the co-flow and fuel jet Reynolds numbers (Re = 5,000/10,000 and 20,000).
- OpenFOAM provides overall more accurate results with respect to Fluent for the current case. This might arise from the highly diffusive nature of the Fluent code. Cases characterized by a more complicated geometry will be analysed in the future.
- The use of non-uniform boundary conditions allows capturing the second radial CO peak, while worsening the CO level along the centerline and close to the axis.

The present study demonstrates the applicability of the Partially-Stirred Reactor model under Moderate or Intense Low oxygen Dilution combustion condition. Various approaches on chemical and mixing time scales evaluation were compared and discussed comprehensively, giving references to the application of Partially-Stirred Reactor model

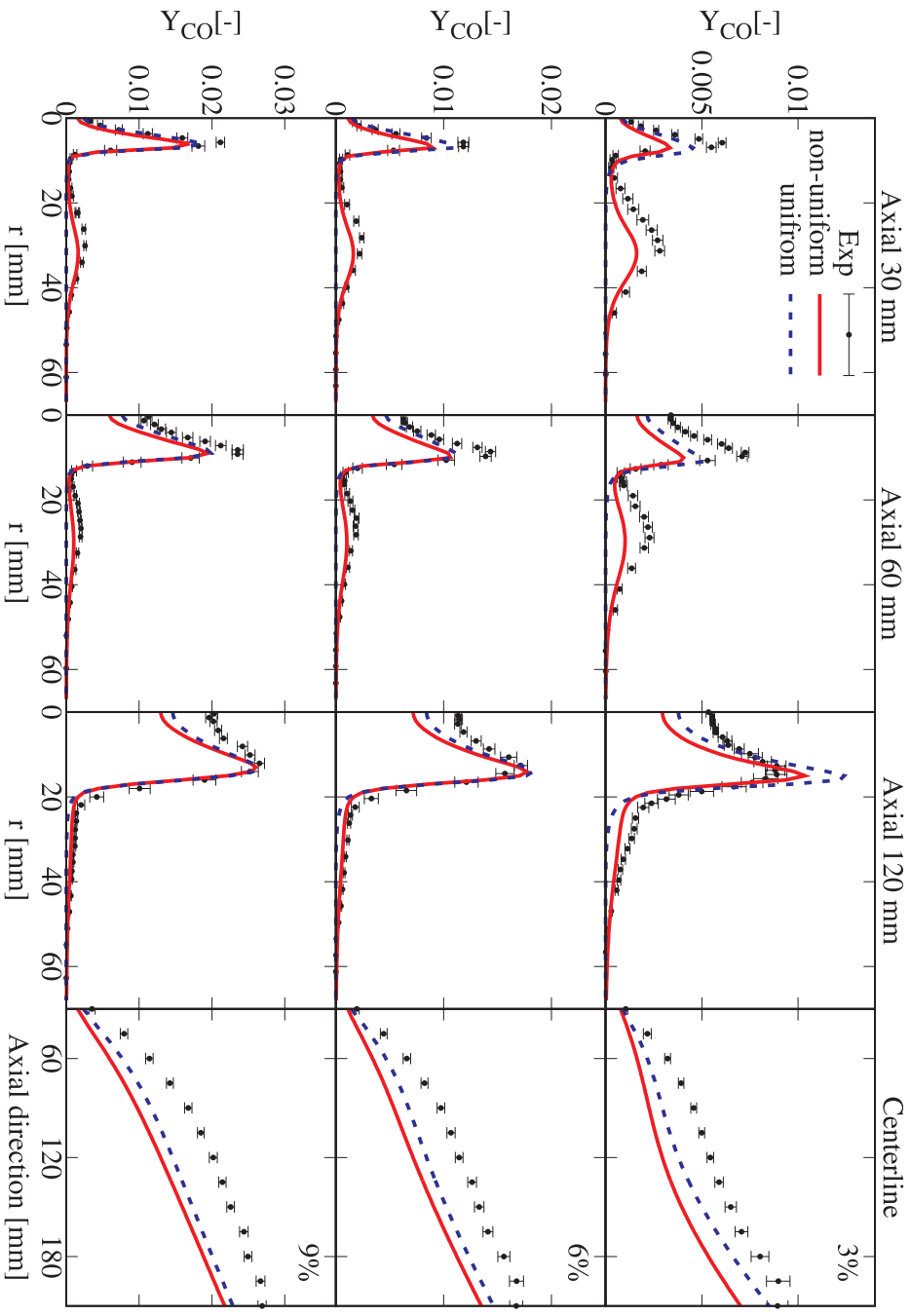

Fig. 20. Mean CO mass fraction profiles obtained using non-uniform and uniform boundary conditions. O_2 mass fraction in the co-flow: 3%, 6% and 9%.

within non-conventional regime. A dynamic model on the estimation of mixing time is evaluated, presenting superior performance than the global models under a wide range of operation conditions. The CPU time required by the dynamic model is comparable with the global ones.

In industrial burners, a wide range of operation conditions exist and the interactions between chemistry and turbulence are complicated because of complex geometry. In this framework, the availability of affordable and accurate numerical tools is the key to unlock the potential of new technologies which are able to deal with a variety of energy vectors, ensuring high efficiency and low pollutant emissions. The present work evaluates a novel implementation of the Partially-Stirred Reactor model, based on the accurate estimation of chemical and mixing time scales. Results show that it has great potentiality for the simulation and development of large scale industrial burners.

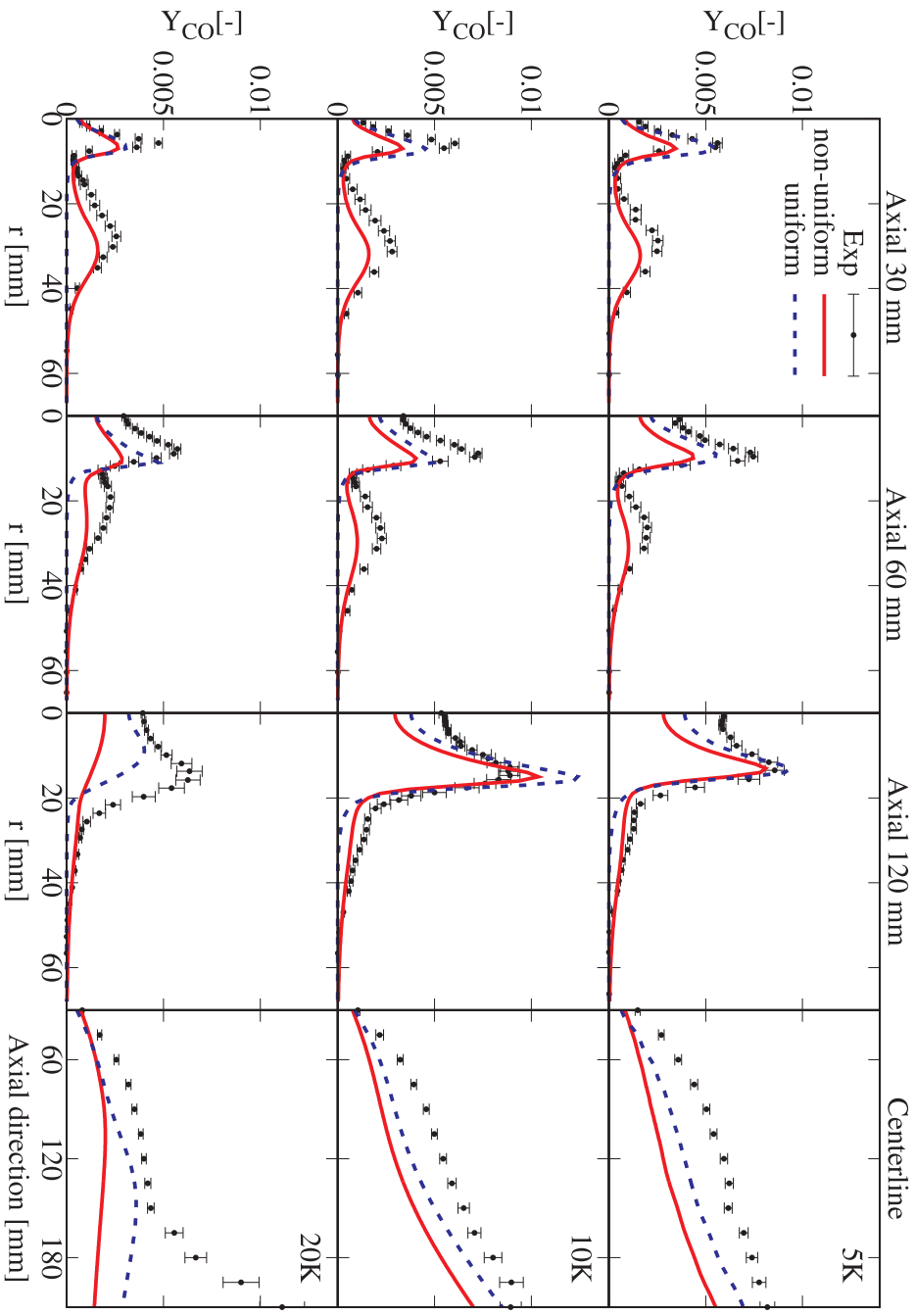

Fig. 21. Mean CO mass fraction profile obtained using the non-uniform and uniform boundary conditions. Fuel jet Reynolds number: 5 k, 10 k and 20 k.

Acknowledgments

This project has received funding from the European Union's Horizon 2020 research and innovation program under the Marie Skłodowska-Curie grant agreement No. 643134. The research of the second author has received funding from the Fonds de la Recherche Scientifique - FNRS Belgium. The research of the last author is sponsored by the European Research Council, Starting Grant No. 714605, and from the Fédération Wallonie-Bruxelles, via 'Les Actions de Recherche Concertée (ARC)' call for 2014–2019.

Appendix A. Supplementary material

Supplementary data associated with this article can be found, in the online version, at http://dx.doi.org/10.1016/j.apenergy.2018.04.085.

References

[1] Wünning JA, Wünning JG. Flameless oxidation to reduce thermal NO-formation. Prog Energy Combust Sci 1997;23:81–94.
[2] Cavaliere A, de Joannon M. MILD combustion. Prog Energy Combust Sci

2004;30:329–66.
[3] de Joannon M, Sorrentino G, Cavaliere A. MILD combustion in diffusion-controlled regimes of hot diluted fuel. Combust Flame 2012;159:1832–9.
[4] Medwell PR, Dally BB. Effect of fuel composition on jet flames in a heated and diluted oxidant stream. Combust Flame 2012;159:3138–45.
[5] Galletti C, Parente A, Tognotti L. Numerical and experimental investigation of a mild combustion burner. Combust Flame 2007;151:649–64.
[6] Parente A, Galletti C, Tognotti L. Effect of the combustion model and kinetic mechanism on the MILD combustion in an industrial burner fed with hydrogen enriched fuels. Int J Hydrogen Energy 2008;33:7553–64.
[7] Xing F, Kumar A, Huang Y, Chan S, Ruan C, Gu S, et al. Flameless combustion with liquid fuel: a review focusing on fundamentals and gas turbine application. Appl Energy 2017;193:28–51.
[8] Cho E-S, Danon B, de Jong W, Roekaerts D. Behavior of a 300 kwth regenerative multi-burner flameless oxidation furnace. Appl Energy 2011;88(12):4952–9.
[9] Cho E-S, Shin D, Lu J, de Jong W, Roekaerts D. Configuration effects of natural gas fired multi-pair regenerative burners in a flameless oxidation furnace on efficiency and emissions. Appl Energy 2013;107:25–32.
[10] Sánchez M, Cadavid F, Amell A. Experimental evaluation of a 20 kW oxygen enhanced self-regenerative burner operated in flameless combustion mode. Appl Energy 2013;111:240–6.
[11] Ye J, Medwell PR, Varea E, Kruse S, Dally BB, Pitsch HG. An experimental study on mild combustion of prevaporised liquid fuels. Appl Energy 2015;151:93–101.
[12] Kruse S, Kerschgens B, Berger L, Varea E, Pitsch H. Experimental and numerical study of mild combustion for gas turbine applications. Appl Energy 2015;148:456–65.
[13] Adamczyk WP, Bialecki RA, Ditaranto M, Gladysz P, Haugen NEL, Katelbach-Wozniak A, et al. CFD modelling and thermodynamic analysis of a concept of a MILD-Oxy combustion large scale pulverized coal boiler. Energy 2017;140(1):1305–15.
[14] Chinnici A, Tian ZF, Lim JH, Nathan GJ, Dally BB. Comparison of system performance in a hybrid solar receiver combustor operating with MILD and conventional combustion. Part II: effect of the combustion mode. Sol Energy 2017;147:478–88.
[15] Minamoto Y, Swaminathan N. Subgrid scale modelling for MILD combustion. Proc Combust Inst 2015;35(3):3529–36.
[16] Chomiak J. Combustion: a study in theory, fact and application. Abacus Press/Gorden and Breach Science Publishers; 1990.
[17] Chomiak J, Karlsson A. Flame liftoff in diesel sprays. Twenty-sixth symposium (international) on combustion. The Combustion Institute; 1996. p. 2557–64.
[18] Golovitchev V, Chomiak J. Numerical modeling of high temperature air flameless combustion. In: The 4th international symposium on high temperature air combustion and gasification; 2001.
[19] Kärrholm FP. Numerical modelling of diesel spray injection, turbulence interaction and combustion, Phd thesis, Chalmers University of Technology, Chalmers, Sweden; 2008.
[20] Nordin PAN. Complex chemistry modeling of diesel spray combustion, Phd thesis, Chalmers University of Technology, Chalmers, Sweden; 2001.
[21] ANSYS®Academic Research, Release 17.0.
[22] Dally BB, Karpetis AN, Barlow RS. Structure of turbulent non-premixed jet flames in a diluted hot coflow. Proc Combust Inst 2002;29:1147–54.
[23] Lysenko DA, Ertesvåg IS, Rian KE. Numerical simulation of non-premixed turbulent combustion using the eddy dissipation concept and comparing with the steady laminar flamelet model. Flow, Turbul Combust 2014;53:577–605.
[24] Parente A, Malik MR, Contino F, Cuoci A, Dally BB. Extension of the eddy dissipation concept for turbulence/chemistry interactions to MILD combustion. Fuel 2015;163:98–111.
[25] Kjäldman L, Brink A, Hupa M. Micro mixing time in the Eddy Dissipation Concept. Combust Sci Technol 2007;154:207–27.
[26] Gonzales M, Borghi R. Turbulent Shear Flows, no. 293-311 in 7. Berlin: Springer Verlag; 1991.
[27] Ferrarotti M, Li Z, Parente A. On the role of mixing models in the simulation of MILD combustion using finite-rate chemistry combustion models. In: 37th international symposium on combustion; 2018. [accepted for presentation].
[28] Raman V, Pitsch H. A consistent LES/filtered-density function formulation for the simulation of turbulent flames with detailed chemistry. Proc Combust Inst 2007;31(2):1711–9.
[29] Ye I. Investigation of the scalar variance and scalar dissipation rate in urans and les, Phd thesis, University of Waterloo, Ontario, Canada, Waterloo, Ontario, Canada; 2011.
[30] Sanders JPH, Gökalp I. Scalar dissipation rate modelling in variable density turbulent axisymmetric jets and diffusion flames. Phys Fluids 1998;10(4):938–48.
[31] Isaac BJ, Parente A, Galletti C, Thornock JN, Smith PJ, Tognotti L. A novel methodology for chemical time scale evaluation with detailed chemical reaction kinetic. Energy Fuels 2013;27(4):2255–65.
[32] Fox RO. Computational models for turbulent reacting flows. Cambridge, UK: Cambridge University Press; 2003.
[33] Li Z, Cuoci A, Sadiki A, Parente A. Comprehensive numerical study of the Adelaide Jet in Hot-Coflow burner by means of RANS and detailed chemistry. Energy 2017;139:555–70.
[34] Ferrarotti M, Galletti C, Parente A, Tognotti L. Development of reduced NOx models for flameless combustion. In: 18th IFRF members conference; 2015.
[35] Oberkampf WL, Barone MF. Measures of agreement between computation and experiment: validation metrics. J Comput Phys 2006;217(1):5–36.
[36] Cuoci A, Frassoldati A, Faravelli T, Ranzi E. Opensmoke+ +: an object-oriented framework for the numerical modeling of reactive systems with detailed kinetic mechanisms. Comput Phys Commun 2015;192:237–64.
[37] Bilger RW, Stårner SH, KEE RJ. On reduced mechanisms for methane-air combustion in nonpremixed flames. Combust Flame 1990;80(2):135–49.
[38] Christo FC, Dally BB. Modelling turbulent reacting jets issuing into a hot and diluted coflow. Combust Flame 2005;142:117–29.
[39] Frassoldati A, Sharma P, Cuoci A, Faravelli T, Ranzi E. Kinetic and fluid dynamics modeling of methane/hydrogen jet flames in diluted coflow. Appl Therm Eng 2009;30:376–83.
[40] Launder BE, Spalding DB. The numerical computations of turbulent flows. Comput Methods Appl Mech Eng 1973;3(2):269–89.
[41] D'Alessandro V, Binci L, Montelpare S, Ricci R. On the development of openfoam solvers based on explicit and implicit high-order Runge-Kutta schemes for incompressible flows with heat transfer. Comput Phys Commun 2018;222(Supplement C):14–30.
[42] Ghasemi A, Roussinova V, Balachandar R, Barron R. Reynolds number effects in the near-field of a turbulent square jet. Exp Therm Fluid Sci 2015;61:249–58.
[43] Russo F, Basse NT. Scaling of turbulence intensity for low-speed flow in smooth pipes. Flow Meas Instrum 2016;52:101–14.
[44] Basse NT. Turbulence intensity and the friction factor for smooth- and rough-wall pipe flow, Fluids 2 (30).